THE ASTROPHYSICAL JOURNAL, 332:964–983, 1988 September 15

STUDIES OF HOT B SUBDWARFS. VI. DETAILED CALCULATIONS OF RADIATIVE FORCES ON METALS IN THE ENVELOPES AND ATMOSPHERES OF HYDROGEN-RICH SUBDWARFS

P. BERGERON, F. WESEMAEL, G. MICHAUD,[1] AND G. FONTAINE[2]
Département de Physique, Université de Montréal
Received 1987 November 30; accepted 1988 March 10

ABSTRACT

Detailed calculations of radiative accelerations on C, N, and Si are presented in model envelopes and atmospheres of hot, hydrogen-rich subdwarf (sdB, sdOB) stars. These calculations are carried out through several levels of approximation in order to examine the sensitivity of $g_{\rm rad}$ to the input physics used. Calculations are first performed in model stellar envelopes, where the radiation flux is estimated with the radiative diffusion approximation. These computations are then extended to optically thin regions, where the Eddington flux is calculated explicitely in LTE. Departures from LTE are also considered, with the help of an approximate treatment of the NLTE ionization balance. The resulting radiative accelerations are estimated to be accurate to better than a factor of ~ 3 in the region of metal line formation. The radiative acceleration profiles are used to calculate a depth-dependent equilibrium abundance profile for C, N, and Si in various models. These can be, occasionally, far from homogeneous and provide a self-consistent input to line profile calculations. Illustrative examples of this procedure are provided.

Radiative accelerations are found to be large enough to counterbalance the efficient gravitational settling of elements in these high-gravity atmospheres. In particular, the radiative support of silicon in the line-forming region of hot ($T_e > 27{,}000$ K) B subdwarfs is strong enough to support large abundances of that element. This result is at odds with several recent analyses of high-dispersion ultraviolet data, which reveal instead a striking underabundance of silicon. This suggests that other particle transport processes operate in the photospheres of hot subdwarfs and compete efficiently with radiative element support. The plausible presence of a weak stellar wind threading the atmosphere, suggested by Michaud *et al.*, is again emphasized.

Subject headings: diffusion — stars: abundances — stars: atmospheres — stars: subdwarfs

I. INTRODUCTION

Analyses of the line spectrum of hot evolved stars, whether white dwarfs or subdwarfs, provide incontrovertible evidence for the presence of abundance anomalies in their atmospheres (Vauclair and Liebert 1987; Shipman 1987). These anomalies can, in principle, be interpreted as the outcome of the often delicate interplay of several physical processes in the outer layers of these stars: convective mixing and dredge-up, accretion, diffusion, and stellar winds have all been called upon in this context.

In the case of hot, hydrogen-rich subdwarfs, current evidence is summarized by Lamontagne, Wesemael, and Fontaine (1987), where the observed C, N, and Si abundance patterns are displayed. To recapitulate briefly, carbon is found to be underabundant over the effective temperature range 20,000–40,000 K covered by the classical hydrogen-rich subdwarfs (as defined, e.g., by Greenstein and Sargent 1974); there is a suggestion that the carbon deficiency might increase with increasing effective temperature. In contrast, nitrogen appears in nearly solar abundance (within a factor of ~ 2) in all objects studied up to now. Finally, silicon reveals a most fascinating pattern: it is observed at an abundance slightly below the solar value at low effective temperatures, but becomes truly underabundant at $T_e \gtrsim 27{,}000$ K, by as much as five orders of magnitude. This large deficiency extends at least up to $T_e \approx 40{,}000$ K. Baschek *et al.* (1982) and Baschek, Höfflich, and Scholz (1982) summarize abundances for several other less abundant ions determined in two bright hydrogen-rich subdwarfs.

Gravitational settling has often been mentioned (Greenstein and Sargent 1974; Baschek and Norris 1975; Winget and Cabot 1980; Kudritzki *et al.* 1982; Wesemael *et al.* 1982) as the source of the long-known and well-documented helium deficiency in these objects (see Heber *et al.* 1984*b* and Heber 1986 for the latest determinations on this subject). Despite the fact that the explanation of the helium abundance pattern might well be more complicated than previously thought (Michaud *et al.* 1988), diffusion processes (including, this time, radiative support) have been immediately, and quite rightly, called upon to explain, at least in qualitative terms, the observed metal abundance anomalies (Baschek *et al.* 1982; Baschek, Höfflich, and Scholz 1982; Heber *et al.* 1984*a*, *b*; Lamontagne *et al.* 1985). The first calculations of abundance anomalies expected from diffusion in hot, hydrogen-rich subdwarfs were performed by Michaud *et al.* (1985, hereafter Paper I). Their computations, which could be claimed to be accurate only *below* the atmosphere, yielded the rather puzzling result that unimpeded diffusion could not lead to the large silicon abundance deficiencies observed in B and OB subdwarfs; in essence, the element support through radiative forces is always intense enough to prevent large deficiencies from developing in the atmosphere. As a possible solution to this riddle, Michaud *et al.* suggested that diffusion might be operating, in hot, hydrogen-rich subdwarfs, in the presence of a competing particle transport process, a weak stellar wind. This result, if confirmed, provides a potentially powerful tool to probe the

[1] Killam Foundation Fellow.
[2] E.W.R. Steacie Memorial Fellow.

hydrodynamics of the outer layers of those stars: the abundances of elements supported by radiative forces would be sensitive to mass loss rates much smaller ($\lesssim 10^{-15}$ $M_{\odot}$ yr^{-1}) than those which can be determined from usual analyses of the line spectrum (Michaud 1986, 1987*a*).

In this paper, we present a study of the radiative support of metals in the outer layers of hot subdwarfs which goes considerably further than our previous investigation. Our motivation is clear: radiative accelerations of ions play a key role in determining the distribution of elements in the outer layers even if other mechanisms, such as winds, are competing with diffusion. Indeed, as demonstrated in Paper I, *the element distribution in an envelope threaded by a weak wind is controlled by the variation of $g_{\rm rad}$ with depth.* Calculations of $g_{\rm rad}$—as accurate and reliable as currently possible—are thus but the first step in a detailed investigation of the hydrodynamics of outer layers of hot subdwarfs.

The need for accurate radiative accelerations *in the atmosphere* is particularly acute for hot subdwarfs. As indicated earlier, radiative acceleration calculations can be claimed to be accurate only below the atmosphere of those stars—a limitation imposed by various approximations made in the calculation of $g_{\rm rad}$ which restrict their applicability to regions where $\tau \gtrsim 1$. How representative are such calculations of the behavior of $g_{\rm rad}$ in the photosphere, the only region accessible to detailed abundance studies? Furthermore, how sensitive are the calculated values of $g_{\rm rad}$ to the various approximations often used in their computations, or to the sometime uncertain atomic physics parameters employed (Michaud 1987*b*)? Detailed calculations of radiative forces in the *atmospheres* of chemically peculiar main-sequence stars are available for a few elements (e.g., Borsenberger, Michaud, and Praderie 1979, 1981, 1984; Alecian and Michaud 1981), but such computations have never been extended to the higher gravities associated with two classes of hot evolved stars with atmospheric abundance anomalies: (1) the hot subdwarf and (2) white dwarf stars.

Motivated by these arguments, we present here the results of our exhaustive study of radiative forces as the source of abundance anomalies in hot, hydrogen-rich subdwarfs. We have taken care, in what follows, to describe accurately the sequence of approximations used at every level of calculations. We first report, in § II, results of calculations of $g_{\rm rad}$ in model envelopes. These are the most common, and most convenient, calculations one can perform. Even then, however, there are at least two distinct levels of approximation in the literature, and their consistency in subdwarf envelopes is investigated. We then move on, in § III, to calculations of $g_{\rm rad}$ in subdwarf atmospheres. There we explore the use of LTE models and, through quantitative calculations, investigate the changes brought about by expected departures from LTE in the ionization balance of the outer stellar layers. These detailed calculations of $g_{\rm rad}$ can be used to compute element equilibrium abundance profiles throughout the atmosphere, and exploratory calculations of this kind are presented in § IV, together with some comments on their relevance to observed abundances.

II. CALCULATION OF $g_{\rm rad}$ IN THE ENVELOPE

a) Basic Ingredients in the Calculation of $g_{\rm rad}$

The traditional way of calculating radiative accelerations in stellar envelopes is described in detail in Vauclair, Michaud, and Charland (1974, hereafter VMC) and in Michaud *et al.* (1976, hereafter MCVV). The main steps are summarized here, where we put the emphasis on the different approximations involved, and on their range of validity.

The radiative acceleration transferred to an element A in the frequency interval $d\nu$ can be written as

$$g_{\rm rad,\,\nu}({\rm A})d\nu = \frac{\kappa_\nu({\rm A})}{X({\rm A})}\frac{4\pi}{c}H_\nu d\nu \tag{1}$$

where κ_ν(A) and X(A) are, respectively, the contribution of element A to the monochromatic opacity, and the mass fraction of the element considered; H_ν is the Eddington flux, and c is the speed of light. When τ_ν, the monochromatic optical depth, is larger than unity, we can make use of the diffusion approximation to the radiation flux (Milne 1927),

$$H_\nu \approx \frac{1}{3}\frac{dB_\nu}{d\tau_\nu} \qquad (\tau_\nu \gg 1)\,, \tag{2}$$

where B_ν is the Planck distribution. With

$$d\tau_\nu = -\rho\kappa_\nu dr\,, \tag{3}$$

and since $B_\nu = B_\nu[T(\tau_\nu)]$, we can rewrite equation (1) as

$$g_{\rm rad,\,\nu}({\rm A})d\nu = \frac{4\pi}{3c}\frac{\kappa_\nu({\rm A})}{\kappa_\nu}\frac{1}{\rho X({\rm A})}\frac{\partial B_\nu}{\partial T}\left(\frac{-\partial T}{\partial r}\right)d\nu\,, \tag{4}$$

which is equation (4) of VMC. In the latter, ρ is the mass density and κ_ν is the total monochromatic opacity including that of element A.

Furthermore, when $\tau_{\rm R}$, the Rosseland mean optical depth, is greater than unity, we can approximate the radiative gradient by

$$\frac{\partial T}{\partial r} = \frac{-3}{16}\frac{\kappa_{\rm R}\rho}{T^3}\frac{R^2}{r^2}T_e^4 \qquad (\tau_{\rm R} \gg 1)\,, \tag{5}$$

where $\kappa_{\rm R}$ is the Rosseland mean opacity, R is the radius of the star, r is the distance from the center of the star, and T_e is the effective temperature. If we combine equations (1)–(5), we find

$$g_{\rm rad,\,\nu}({\rm A})d\nu = 7.27\times10^{-17}\frac{R^2}{r^2}T_e^4\frac{\kappa_\nu({\rm A})}{\kappa_\nu}\frac{\kappa_{\rm R}}{X({\rm A})}u^4\frac{e^u}{(e^u-1)^2}du\,, \tag{6}$$

where $u \equiv h\nu/kT$. Equation (6) is valid and formally exact as long as both τ_ν *and* $\tau_{\rm R}$ are greater than unity. The computation of the total radiative acceleration formally requires an integration over frequency of equation (6), and also a knowledge of the relevant atomic data needed to evaluate the opacities. Because the latter can be cumbersome to calculate, one sometimes prefers to use the following approximation.

b) The MCVV Approximation

MCVV demonstrate that, under certain circumstances, equation (6) can be simplified considerably. We first consider the maximum radiative acceleration which occurs when the lines are completely unsaturated; $g_{\rm rad}$ can then be expressed as

$$g_{\rm rad}^{\rm max} = 1.7\times10^{-4}\frac{R^2}{r^2}\frac{T_e^4}{TA}\ {\rm cm\ s^{-2}}\,, \tag{7}$$

where A is the atomic mass number of element A. Among the successive approximations needed to reach equation (7), we note the following: since most of the radiative support comes from a broad energy interval around the flux maximum, κ_ν and

$\partial B_\nu/\partial T$ can be replaced by constants in that interval. A first correction to this maximum value of $g_{\rm rad}$ is introduced to take into account the case when the electronic orbital configuration is that of a noble gas. Because of the large excitation energies associated with these stable configurations, the resulting radiative acceleration is significantly reduced. Equation (7), corrected for rare gas configuration if necessary, still overestimates the radiative acceleration when the lines are saturated. This reduction in radiative support can be taken into account by applying a suitable correction factor, which was obtained by MCVV from a detailed integration of equation (6) on each level of Mn I–V configurations (Moore 1949). From this detailed calculation, $g_{\rm rad}$ (again corrected for rare configuration if necessary) is fitted by an approximate analytical expression which depends only on T, $\kappa_{\rm R}$, the mass and the fractional abundance of the element considered. After appropriate scaling, this fit is applied to other elements as well (see Appendix C of MCVV for details). Finally, because of the simultaneous presence of many ionization states having different diffusion velocities, some care must be taken when summing their respective contributions. Following the prescription of Montmerle and Michaud (1976), we write the total radiative acceleration as an average of the respective contribution of each ionization state weighted by the appropriate population fractions, diffusion coefficients, and ionization probability by both collisional and radiative processes (see their eq. [18]). The final expression is written in a compact form in which the detailed structure of the atomic levels and transitions are replaced by statistical estimates of the oscillator strengths, as described in Appendix A of MCVV. We confront here this approximate treatment with the following detailed calculation. In both cases, the contribution of the continuum to the radiative acceleration is negligible and has thus not been incorporated in our calculations (see § II*c* of MCVV).

c) The Detailed Calculation of $g_{\rm rad}$

The alternate formalism used here is described in Michaud, Vauclair, and Vauclair (1983, hereafter MVV), where it is used to compute $g_{\rm rad}$ on beryllium and carbon in horizontal-branch stars. We return to equation (6) and write *explicitly* the monochromatic opacity of element A as

$$\kappa_\nu({\rm A}) = \frac{\pi e^2}{mc} \sum_{ij} \frac{N_{ij}}{\rho} \sum_k f_{i,j-k}\,\phi_\nu\,, \tag{8}$$

where the sum extends over the ionization states i, and the excitation levels j and k. The population N_{ij} is calculated in LTE through the usual Saha and Maxwell-Boltzmann equations. The oscillator strengths $f_{i,j-k}$ are taken from the tables of Wiese, Smith, and Glennon (1966), Wiese, Smith, and Miles (1969), and—when unavailable—from the estimates of Appendix A of MCVV (the so-called middle approximation).

All transitions permitted by selection rules are included. The line profile ϕ_ν is a Voigt profile which combines natural width and pressure broadening calculated using equation (3.1) of MVV. Finally, the frequency-dependent radiative acceleration (our eq. [6]) is integrated numerically for each line of each state of ionization, with the average over ionization states performed as in the preceding section. Within these improved calculations, the main uncertainties reside in the pressure broadening parameters γ_p, which can be quite poorly known. For example, the constant appearing in equation (3.1) of MVV for γ_p was obtained by requiring that, on the average, this expression agree with the calculations of Chapelle and Sahal-Bréchot (1970) and Sahal-Bréchot and Segre (1971). However, the constant derived by Cox (1965), which is obtained through the hydrogenic approximation, is about 10 times larger. To reflect this uncertainty in the appropriate value of γ_p, we have calculated two distinct sets of radiative accelerations in envelope models: one with the value of MVV, and one with γ_p increased by a factor of 10. It is worth noting that in the case of unsaturated lines, the exact value used is irrelevant (see e.g., § III*a* of MVV).

d) Results

We calculate radiative accelerations on C, N, and Si in envelope models which have physical parameters representative of the classical hot, hydrogen-rich subdwarfs. We use a code similar to that of Paczyński (1969), as adapted by Martel (1973). The models considered have effective temperatures of T_e = 20,000 K, 35,000 K, and 50,000 K with, for each temperature, gravities of $\log g$ = 5.0, 5.5, and 6.0. The mass fractions of helium and metals used in the construction of the envelope models are, respectively, 10^{-2} and 10^{-4}. Their exact values are of little importance for the model stratification. For the calculation of $g_{\rm rad}$ in these envelope models, the continuous opacity is evaluated with equation (8) of Borsenberger, Michaud, and Praderie (1979), while $\kappa_{\rm R}$ is interpolated in the tables of Cox and Stewart (1970) and Paczyński (1969). In the figures which follow, each such model will be referred to by a specific number which reflects its physical parameters. These numbers are given in Table 1.

The main results of this section are displayed on Figures 1–3. On each, the solid line represents the so-called detailed calculation (see § II*c*), while the dashed line represents the same approximation but with the pressure width arbitrarily increased by a factor of 10, as discussed above. The dash-dotted line is the MCVV approximation described in § II*b*. In these, and other similar plots, the horizontal dashed line represents g_E, the local gravity corrected for the local electric field (see eq. [13] and Montmerle and Michaud 1976). In this set of calculations, the initial abundance profiles are homogeneous and correspond, for each element, to the solar value. In the regions where $g_{\rm rad}$ exceeds g_E, the element is radiatively supported and accumulates. This accumulation will, in turn, increase the line saturation. As seen previously, the radiative acceleration will then decrease until an equilibrium is reached between $g_{\rm rad}$ and g_E. Inversely, if $g_{\rm rad} < g_E$, the element will sink into the star. However, this abundance decrease may or may not lead to an increase in the local value of $g_{\rm rad}$. If the lines are already unsaturated, no further increase in $g_{\rm rad}$ will be achieved, and $g_{\rm rad}$ will remain smaller than g_E. In this case, the

TABLE 1

PHYSICAL PARAMETERS OF MODELS

T_e(K)	$\log g$	Model Number
20,000	5.0	2050
	5.5	2055
	6.0	2060
35,000	5.0	3550
	5.5	3555
	6.0	3560
50,000	5.0	5050
	5.5	5055
	6.0	5060

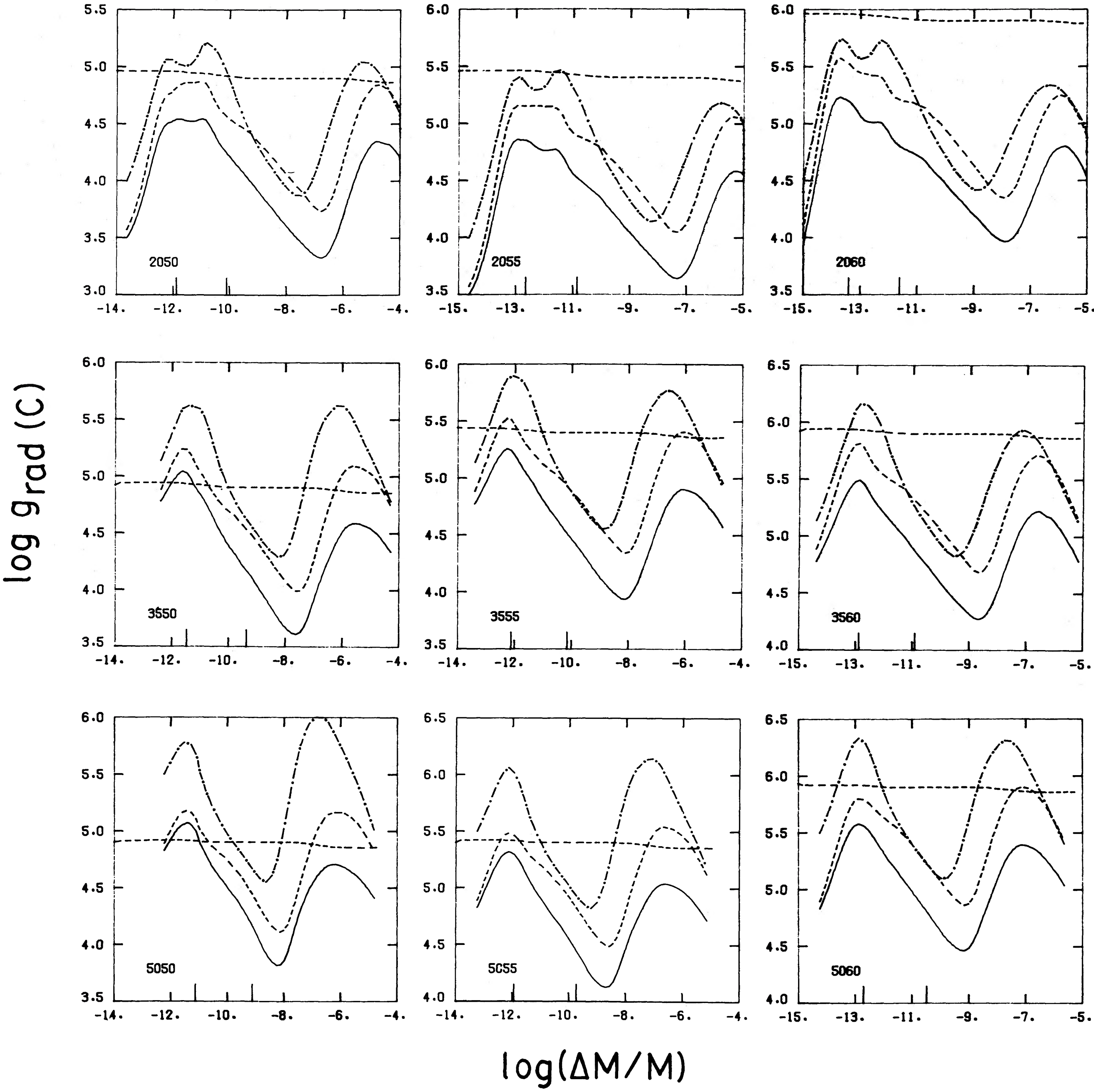

FIG. 1.—Radiative accelerations on carbon for a solar abundance as a function of fractional mass in the envelopes of hot, hydrogen-rich subdwarfs. Each figure is labeled by a number which gives the physical parameters of the model (see Table 1). The solid lines represent the detailed calculation performed as described in § II*c* while the dashed lines represent the same calculation but with pressure widths increased by a factor of 10. The dash-dotted lines show the results obtained with the MCVV approximation described in § II*b*. The horizontal dashed lines indicate the local value of the gravity corrected for the effects of the electric field. Rosseland mean optical depths of 1 and 100 are indicated by long tick marks on the horizontal axis.

local abundance is determined by the concentration gradient. If the lines are initially saturated, however, a decrease in the abundance will indeed lead to an increase in $g_{\rm rad}$. We defer further discussion of these effects to § IV, where a calculation of equilibrium composition profiles for several elements in the atmospheres of hot subdwarfs will be presented.

Our results confirm the expected importance of radiative acceleration on C, N, and Si in the envelopes of hot, hydrogen-rich subdwarfs. More particularly, C, N, and Si are always supported near their solar abundances in the line-forming regions (except perhaps for C in some of our models). It is also clear that the approximate treatment of MCVV is in good qualitative agreement with the more detailed calculation. However, the MCVV formalism generally overestimates the value of $g_{\rm rad}$, especially in the deep regions of models at high effective temperatures. But in the line-forming regions, this

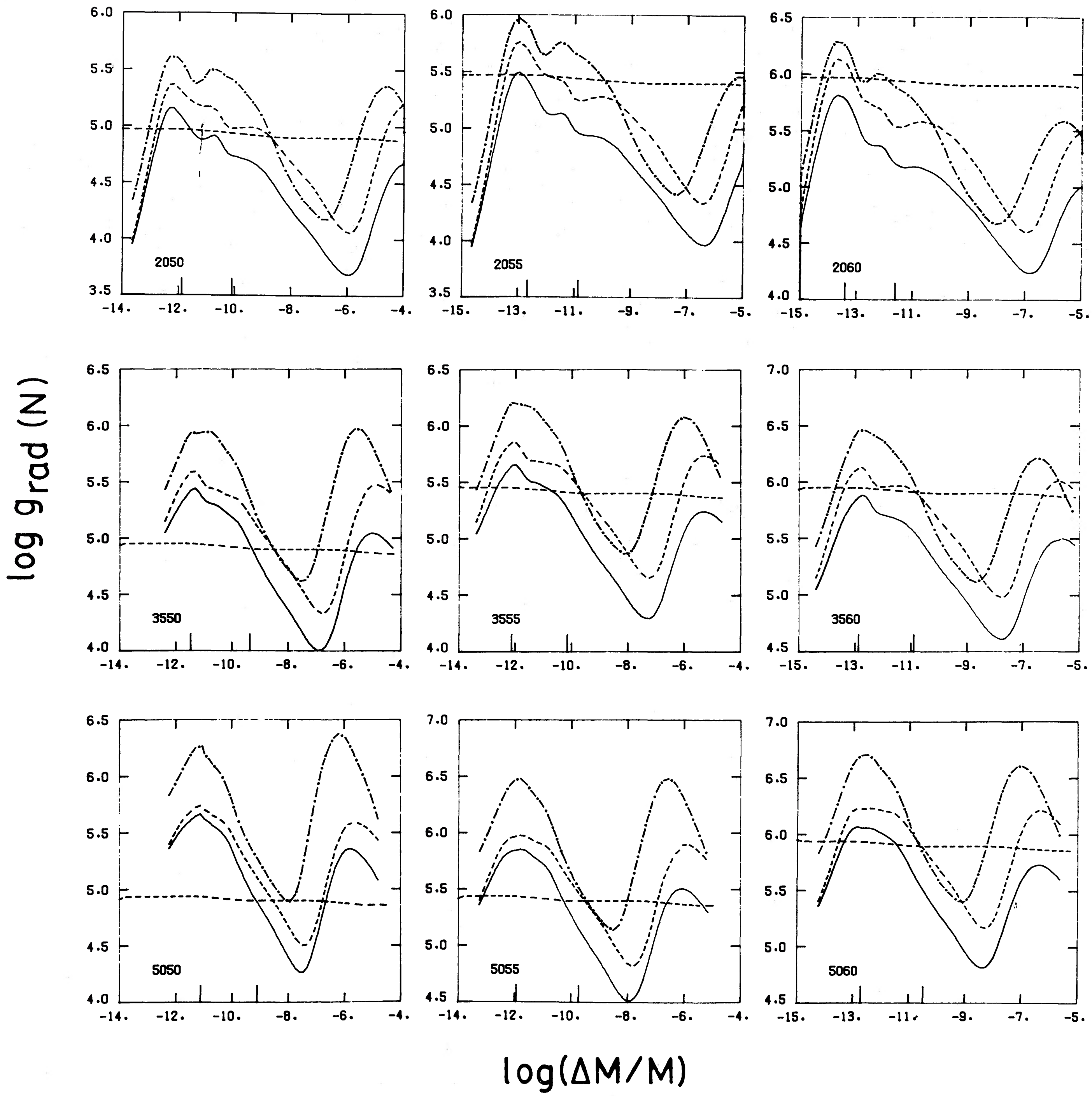

FIG. 2.—Same as Fig. 1, but for nitrogen

overestimate is never larger than a factor of ~ 3. The MCVV formalism also differs from the detailed calculation in the exact location of the large dip on each curve caused by the noble gas configuration. Nevertheless, our calculations indicate that this approximate formalism is a reliable measure of the expected radiative element support in the envelopes of these stars and can probably be applied to other elements as required in the future. It is also clear from Figures 1–3 that the uncertainty in the pressure-broadening parameter γ_p is not critical. An increase by a factor of 10 in γ_p yields an increase in $g_{\rm rad}$ by less than a factor of ~ 2 in the line-forming region.

It is possible to obtain the approximate equilibrium abundance, N_e, with an appropriate scaling of Figures 1–3 given by $N_e = N_0(g_{\rm rad}/g_E)^2$, where N_0 is the initial abundance (solar in our case). This expression reflects the approximate $N^{-1/2}$ dependence of $g_{\rm rad}$ when line saturation is important (see, e.g., MCVV and Vauclair, Vauclair, and Greenstein 1979). With this in mind, one can generalize the conclusions of Paper I,

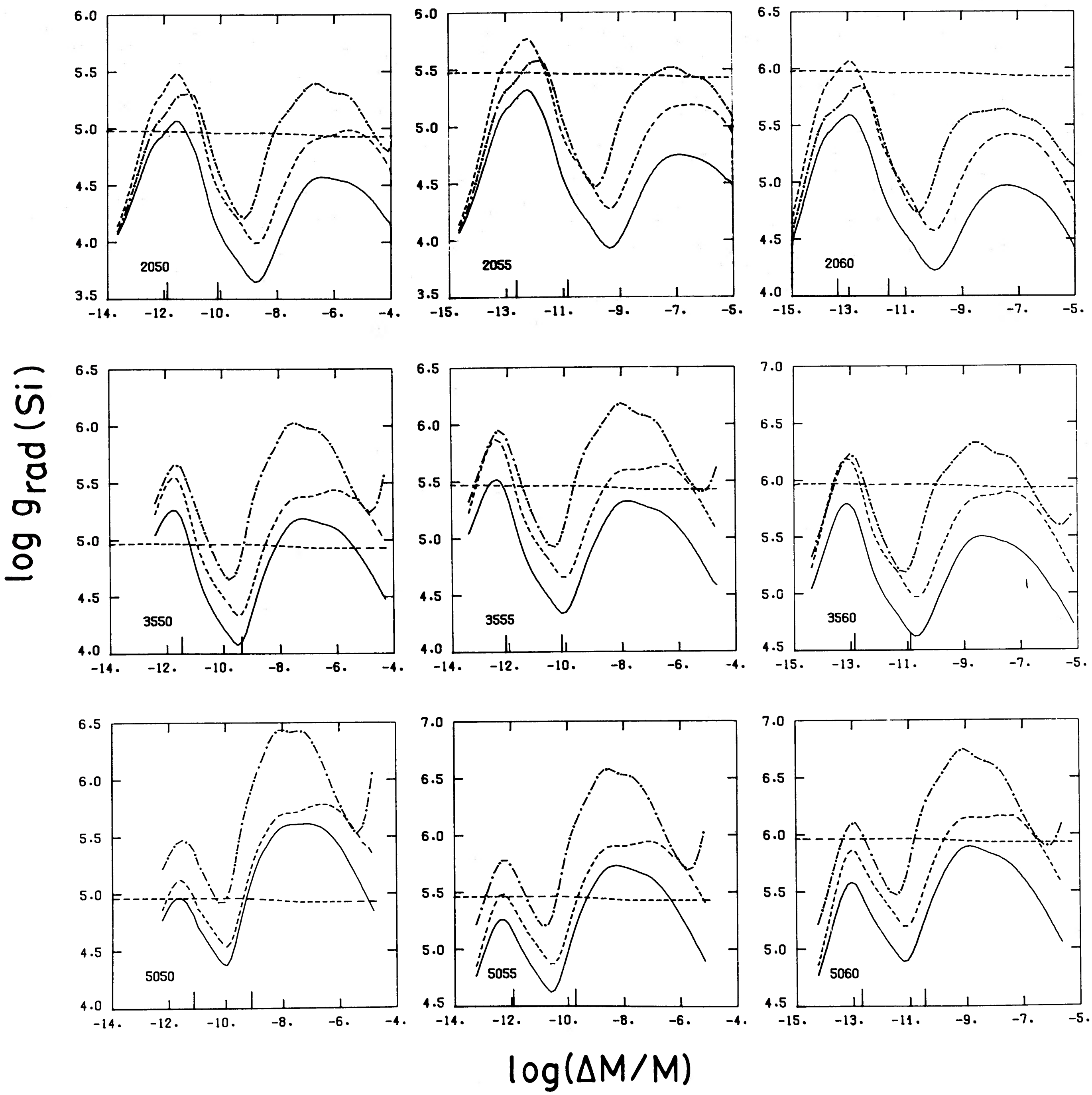

FIG. 3.—Same as Fig. 1, but for silicon

where a single model at 35,000 K, log $g = 5.5$ was presented and discussed. In particular, it is clear that abundances of silicon larger than ~ 0.1 times the solar value are predicted to be supported throughout the classical hydrogen-rich subdwarf domain, as the radiative acceleration on silicon is never more than a factor of 3 smaller than the gravitational acceleration for an initial abundance at the solar value.

III. CALCULATION OF g_{rad} IN THE ATMOSPHERE

a) The Need for Model Atmospheres

In order to perform the comparison of observed abundances with theoretical predictions from element diffusion calculations, improved radiative force computations must be obtained in the atmospheric regions where the lines are formed. This requires realistic model atmospheres because envelope codes do not give the accurate thermodynamic stratification needed in the optically thin regions. We have therefore used model atmospheres similar to those described by Wesemael *et al.* (1980), which are in LTE and are hydrogen-line–blanketed. The good agreement in the physical parameters at the junction between the completely independent envelope and atmosphere calculations can be appreciated from Figure 4 where we show the gas pressure, temperature, and Rosseland mean opacity stratification in both an envelope and an atmo-

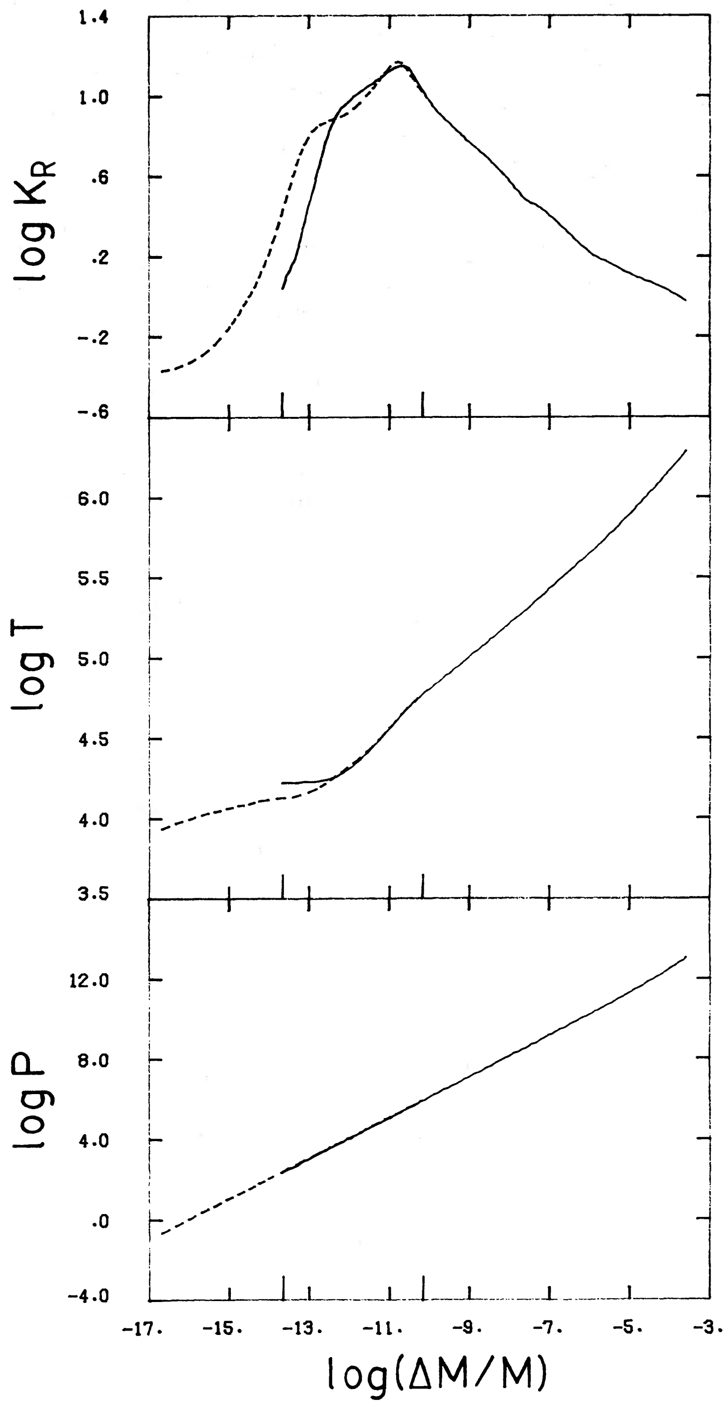

FIG. 4.—Gas pressure, temperature, and Rosseland mean opacity stratification in both an envelope (*solid line*) and an atmosphere model (*dashed line*) at $T_e = 20{,}000$ K, log $g = 5.0$. Also indicated by long tick marks on the vertical axis are the regions where the envelope model begins and where the atmosphere model ends.

sphere model at $T_e = 20{,}000$ K, log $g = 5.0$. Perhaps a more instructive investigation of this matching at the boundaries can be made by computing radiative accelerations in the atmosphere with the detailed calculation described in § II*c*, and then comparing those with the same calculations, but carried out in the envelope. It should be stressed, however, that only in the atmospheric calculation of $g_{\rm rad}$ are both $\kappa_{\rm R}$ and κ_ν explicitly calculated, and that, in both cases, the radiative diffusion approximation is used. An illustrative example is presented in Figure 5 for carbon in a few selected models. The close agreement between the two sets of calculations is encouraging. The atmospheric part of these curves will be referred to below as the atmospheric radiative-diffusion (ARD) calculation.

b) *Detailed Solution for the Radiative Flux*

The extension of our calculations to atmospheric models permits some of the most doubtful approximations of envelope calculations to be dropped. In particular, the radiative-

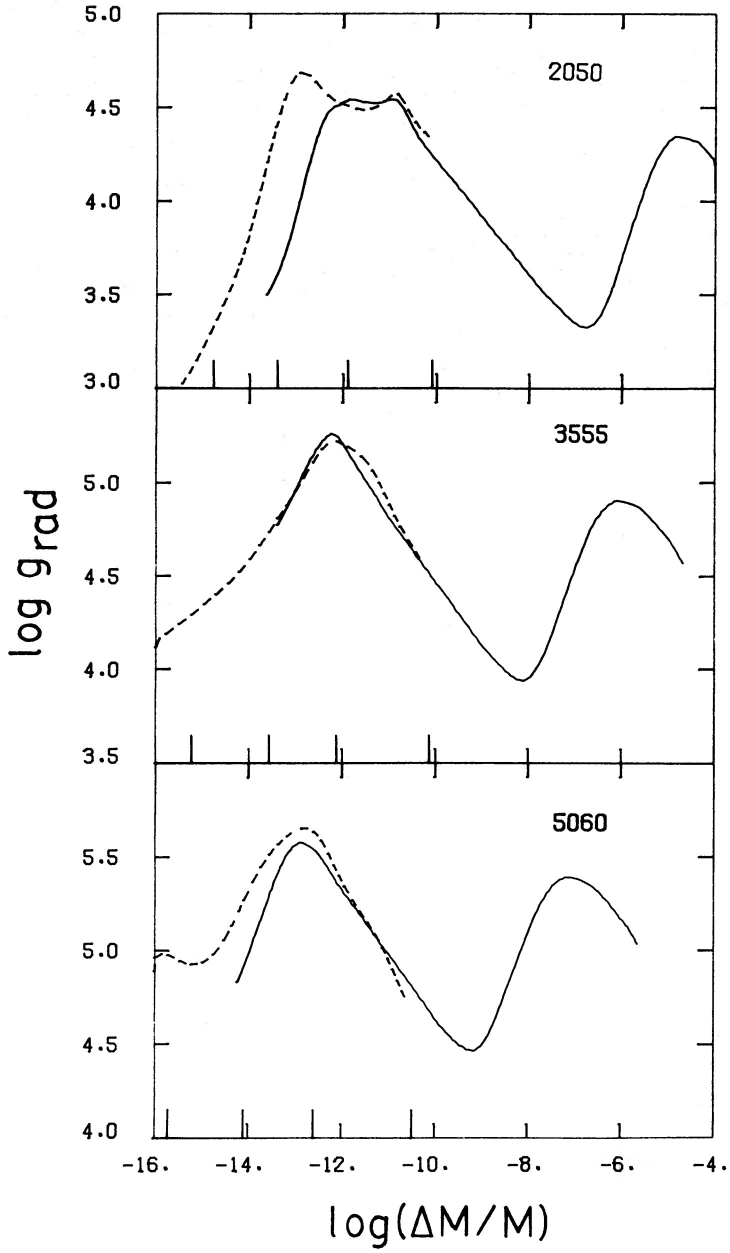

FIG. 5.—Radiative accelerations on carbon for a solar abundance in both the envelope (*solid line*) and the atmosphere (*dashed line*) of three representative models using the detailed calculation described in § IIc. Rosseland mean optical depths of 10^{-4}, 10^{-2}, 1, and 10^2 are also indicated by long tick marks on the horizontal axis.

diffusion approximation is removed and, instead, we solve explicitely the equation of radiative transfer in the atmosphere with the Feautrier method: The specific intensity $I_\nu(\mu)$ is written in terms of $P_\nu(\mu)$ and $R_\nu(\mu)$,

$$P_\nu(\mu) = \tfrac{1}{2}[I_\nu(+\mu) + I_\nu(-\mu)] , \tag{9a}$$

$$R_\nu(\mu) = \tfrac{1}{2}[I_\nu(+\mu) - I_\nu(-\mu)] . \tag{9b}$$

The Eddington flux is obtained from the second order moment of the radiation field K_ν,

$$H_\nu = \frac{dK_\nu}{d\tau_\nu} , \tag{10}$$

where K_ν is given by

$$K_\nu = \tfrac{1}{2} \int_{-1}^{1} I_\nu(\mu)\mu^2 \, d\mu = \int_0^1 P_\nu(\mu)\mu^2 \, d\mu . \tag{11}$$

One can then readily go back to equation (1) and integrate numerically each line and sum their contributions, as done previously. In doing this, we consider that the continuum opacity is constant across the width of the line, and that no superposition of lines from trace elements occurs. We have, however, fully taken into account the occasional overlap of some metal lines with members of the Lyman series of hydrogen. Our LTE results are presented in Figures 6–8. Exami-

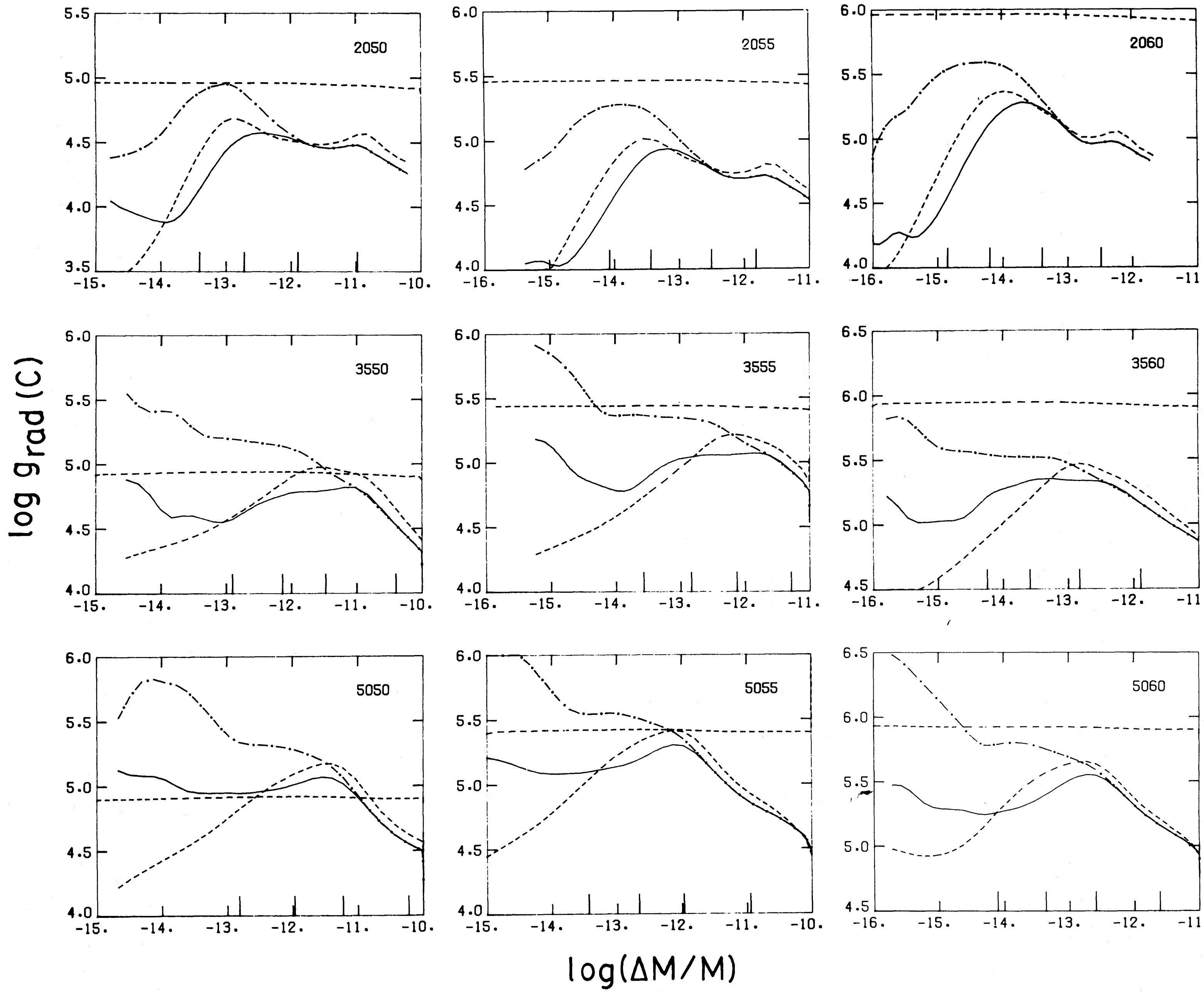

FIG. 6.—Radiative accelerations on carbon for a solar abundance in the atmospheres of hot, hydrogen-rich subdwarfs. The dashed lines represent the calculation performed using the atmospheric radiative-diffusion (ARD) approximation described in § II*b*. The two other curves show the results obtained by explicitly calculating the radiative flux in LTE (*dash-dotted lines*) and with our approximate NLTE treatment (*solid lines*). Rosseland mean optical depths of 10^{-2}, 10^{-1}, 1, and 10 are indicated by long tick marks on the horizontal axis.

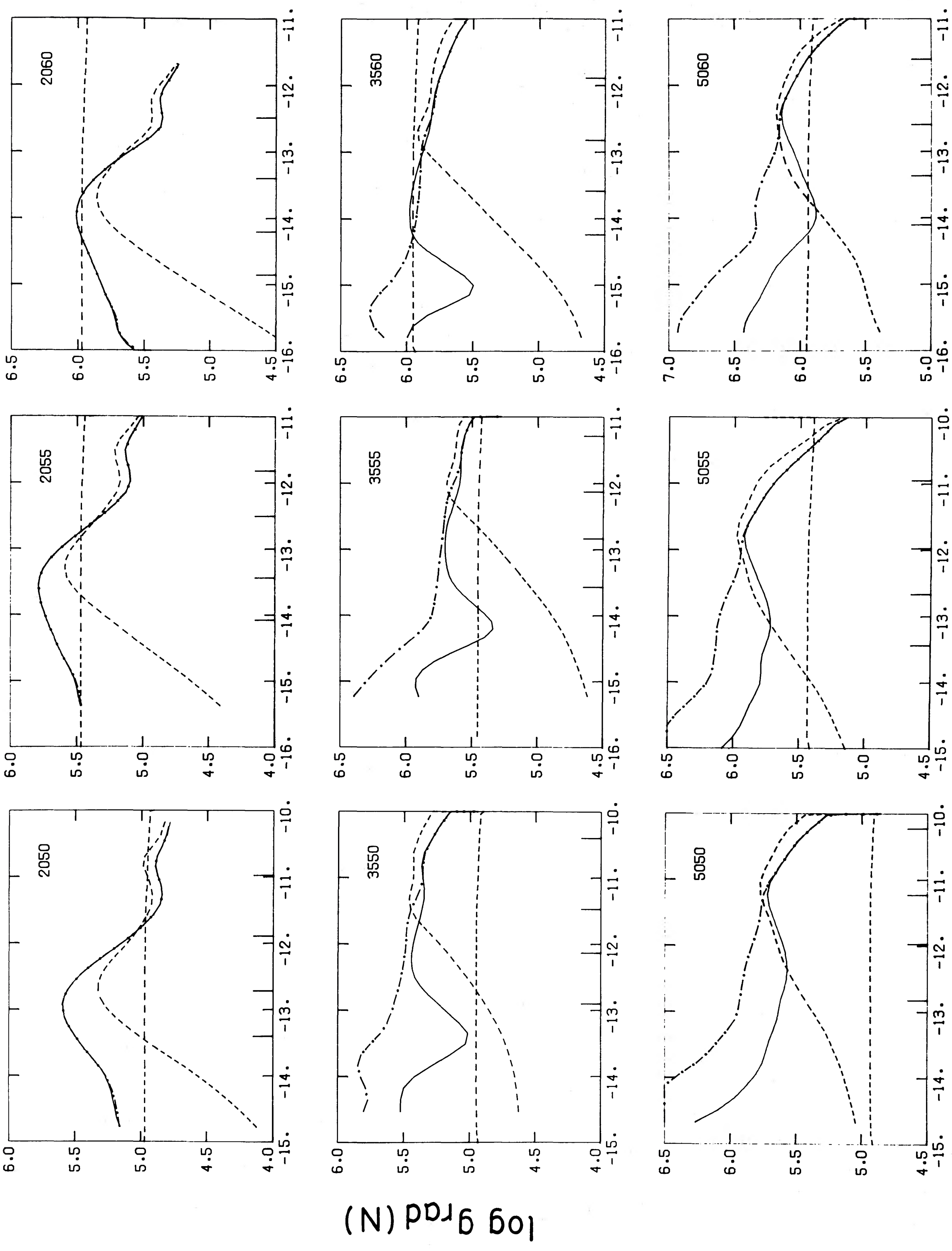

FIG. 7.—Same as Fig. 6, but for nitrogen

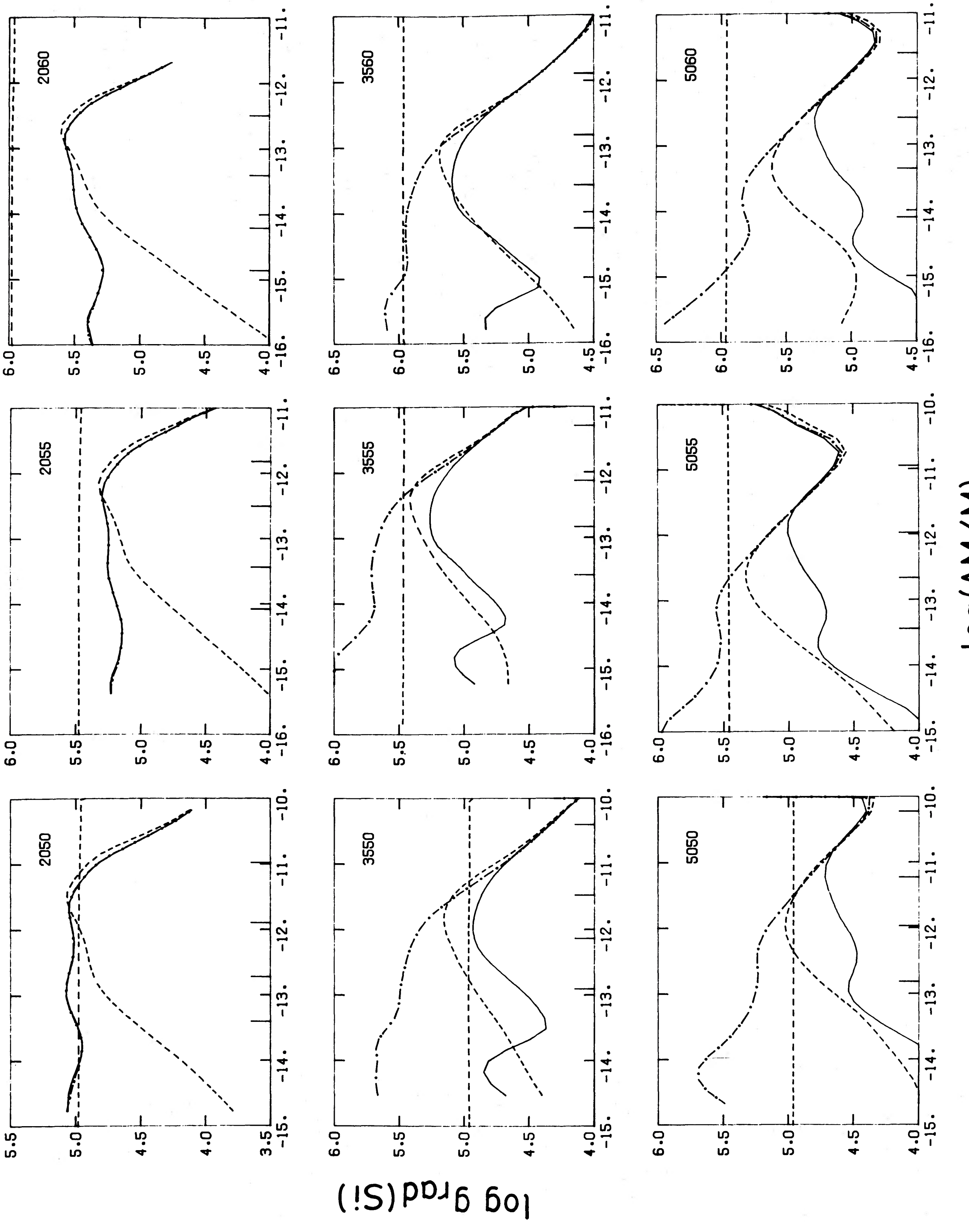

FIG. 8.—Same as Fig. 6, but for silicon

nation of these figures shows that the detailed solution of the radiative flux greatly increases $g_{\rm rad}$ compared to its value obtained within the radiative-diffusion approximation. This is a direct consequence of the increase in the monochromatic flux at the wavelengths where important lines are found. In some cases, $g_{\rm rad}$ keeps increasing toward the surface at a value larger than the local gravity g_E, a result which suggests that the element might not remain bound to the star. However the calculation of $g_{\rm rad}$ at such low optical depths remains uncertain because of potential NLTE effects, and further refinements must be included in the computation of $g_{\rm rad}$ before a conclusive statement can be made on the behavior of specific elements in the outermost stellar layers.

c) A NLTE Approach to the Ionization Equilibrium

In the optically thin layers of LTE atmosphere models, the decrease of the electronic temperature with decreasing optical depth forces the elements to recombine, since the ionization equilibrium is governed by the Saha equation. In terms of radiative acceleration, this results in the increase of $g_{\rm rad}$ observed in the optically thin layers of Figures 6–8. However, in such low-density regions, photoionizations dominate over collisional ionizations because of the strong radiation field; the ensuing decoupling of the ionization balance from the local temperature produces departures of the occupation numbers from those obtained in LTE. NLTE calculations are thus needed for our purpose, but remain generally unavailable for large grids of models covering the subdwarf domain (the work of Michaud *et al.* 1988 being a recent exception). To overcome this situation, we made use of the following approximate treatment to the NLTE solution: instead of solving the complete set of statistical equilibrium equations, we use a radiation temperature instead of the usual electronic temperature in the Saha equation. The justification for this substitution is based on the fact that, because of the transparency of the atmosphere, photons at a particular depth may originate from deeper regions where the temperature is much higher than the local temperature; the ionization equilibrium is thus shifted to higher states if the temperature stratification is a monotonic increasing function of depth. For a particular transition between two successive states of ionization, the ionizing photons will thus have a radiation temperature representative of the local temperature of the regions where they originate. Accordingly, we first identify, for each ionization state, the threshold frequency associated with the ground level; we then find, at each depth, the radiation density at that frequency. This density is then equated to a Planck function, from which we extract the radiation temperature which is then inserted in the Saha equation. Further arguments and details on this method can be found in Mihalas (1978, p. 123 f.). The final approximate ionization equation is given by

$$\frac{n_e n_{0\,j+1}}{n_{0,j}} = \frac{2g_{0,j+1}}{g_{0,j}} \left(\frac{2\pi mkT_r}{h^2}\right)^{3/2} \left(\frac{T_e}{T_r}\right)^{1/2} \exp\left(\frac{\chi_{Ij}}{kT_r}\right), \quad (12)$$

where $n_{0,j}$ and $g_{0,j}$ are respectively the population number and statistical weight of the ground state of the ionization state j, T_e is the electronic temperature (not the effective temperature), T_r is the radiation temperature, and χ_{Ij} is the ionization potential measured from the ground state. Other symbols have their usual meaning. In our procedure, the thermodynamic stratification is kept in LTE; only the trace element considered has been allowed to depart from LTE. The different excitation equilibrium populations are still calculated by the Maxwell-Boltzmann equation. We realize this procedure is only a rough approximation to a full NLTE analysis. However, detailed calculations indicate that departures from LTE affect more directly the ionization balance than the excitation balance (see, e.g., Gigas 1986, 1988). The evaluation of excitation in LTE thus appears more justified.

A further check on the validity of equation (12) can be made through a comparison with the detailed NLTE ionization equilibrium abundances obtained by Kamp (1973) in his study of silicon line formation in early-type main-sequence atmospheres. In that work, fractional populations of each state of ionization of Si were calculated in model atmospheres from the set of Auer and Mihalas (1972). Qualitative comparisons of these detailed calculations with some carried out with the approximate treatment discussed here show good agreement and indicate that our method reproduces satisfactorily the ionization equilibrium shift produced by NLTE effects. A final test of this approximate NLTE treatment is provided by a study of detailed NLTE radiative accelerations on helium in the atmospheres of sdOB stars (Michaud *et al.* 1988), where we show that, for that element, the approximate NLTE calculation of $g_{\rm rad}$ follows the detailed NLTE calculation in the line-forming regions.

We present in Figures 6–8 these approximate NLTE calculations in our grid of models. Detailed study of the ionization equilibrium reveals that ionization proceeds according to intuition: in the LTE approximation, strong recombination occurs in the upper atmosphere, while the NLTE treatment, the strong radiation field further ionizes the element considered. A decrease of $g_{\rm rad}$ (NLTE) compared to $g_{\rm rad}$ (LTE) is thus produced in the optically thin layers. Not unexpectedly, in the deeper regions, where LTE is recovered, both formalisms agree, and match generally well the ARD approximation discussed in § III*a*. Of course, below the atmosphere, both LTE and the radiative-diffusion approximation are adequate. Further examination reveals that, occasionally, $g_{\rm rad}$ (NLTE) itself closely resembles the ARD approximation. This is merely a coincidence: indeed, in these cases, the increase of $g_{\rm rad}$ found by solving for the exact radiative flux and its decrease brought about by the approximate NLTE treatment nearly cancel each other in the optically thin regions. Another noteworthy behavior is that of nitrogen and silicon in the models at 20,000 K, where the calculation of $g_{\rm rad}$ (LTE) and $g_{\rm rad}$ (NLTE) give identical results. At this temperature, the continuum opacity of hydrogen is large enough for the mean free path of the ionizing photons to be very small. Hence, in our procedure, the radiation temperature is almost equal to the local electronic temperature. In contrast, for carbon, the main contribution to $g_{\rm rad}$ (LTE) in the atmosphere comes from C I which has a threshold ionization frequency ($\lambda = 1100$ Å) on the low-frequency side of the Lyman jump. The radiation temperature is thus higher than the local temperature, C I ionizes to C II, and the total radiative acceleration is thereby reduced. In models at 50,000 K, the NLTE results are generally intermediate between $g_{\rm rad}$ (LTE) and the ARD approximation except for silicon. For the latter, $g_{\rm rad}$ (NLTE) is significantly smaller than the value obtained with the ARD approximation, even at $\tau_{\rm R} = 1$ where both formalisms are usually in accord. This reflects the increasingly low opacity in the hydrogen continuum which, for the particular case of silicon, favors the noble gas configuration. Our approximate NLTE calculations of $g_{\rm rad}$ represent the best estimates currently available of radiative accelerations of metals in hot subdwarfs and can now be used to compute equilibrium abundance profiles in the atmosphere.

IV. CONFRONTATIONS WITH OBSERVATIONS

a) Equilibrium Abundance Profiles

The diffusion velocity of a trace ion of charge Z and atomic mass A in a fully ionized hydrogen plasma is given by

$$v_D = D_{12}\left[\frac{-\partial \ln c}{\partial r} - \left(A - \frac{Z}{2} - \frac{1}{2}\right)\frac{m_p g}{kT} + \frac{A m_p g_{\rm rad}}{kT}\right], \quad (13)$$

where c is the element concentration, m_p is the proton mass, and D_{12} is the atomic diffusion coefficient. Thermal diffusion is neglected here, as its effects are relatively small in stellar atmospheres (Paquette *et al.* 1986).

Equilibrium is achieved when the diffusion velocity vanishes everywhere in the atmosphere and envelope. Under such circumstances, the composition profile can be determined. It is a good approximation to neglect the contribution of the first term in brackets, the concentration gradient. We have verified, *a posteriori*, its relative unimportance with respect to the other two terms of equation (13). It is found that in all cases, concentration gradients are negligible so that the equilibrium profile is simply found by setting the sum of the last two terms of equation (13) equal to zero.

Because $g_{\rm rad}$ is dependent on the concentration, a grid of $g_{\rm rad}$ for different homogeneous abundance profiles has been constructed, and an interpolation in this grid is used. Such grids are presented in Figure 9 for some typical cases. The procedure consists in finding at each depth, the concentration which yields a value of $g_{\rm rad}$ which counterweights exactly the gravitational term of equation (13). Although this procedure is accurate in the deep atmospheric regions, small departures from the true equilibrium profile may occur in the upper atmosphere. In the deep regions, the radiative acceleration depends only on the local concentration of the element. The small mean free path of photons thus decouples the radiative flux at one depth from the concentration at another depth. At small optical depths, however, radiative transfer effects prevent such complete decoupling. The resulting deviations from the equilibrium profile, which remain small, are ignored here.

Figures 10–12 display these equilibrium profiles for C, N, and Si for our grid of model atmospheres. The shape of the silicon profile is markedly different from that of the other two elements in the hotter models. The reason for this contrasting behavior is that the lines of carbon and nitrogen are saturated throughout the atmospheric regions; it is then possible to adjust the abundance until the radiative acceleration balances the local gravity (see § II*d* and also Fig. 9). In the case of silicon in the hotter models, however, we find that, even when its abundance is so low that the lines are unsaturated in the uppermost atmosphere, the radiative acceleration is always smaller than the local gravity: silicon is thus not supported in the optically thin regions, and neither is it much deeper in the atmosphere.

The situation considered here is one where equilibrium is reached everywhere in the outer layers between downward settling and upward radiative support. This is the parameter-free model discussed by Michaud (1977) for the chemically peculiar main-sequence stars. Clearly, the ultimate test of the relevance of our equilibrium abundance profiles and, in a broader sense, of the parameter-free model for hot subdwarfs, rests with a comparison with observations. This is a complex problem,

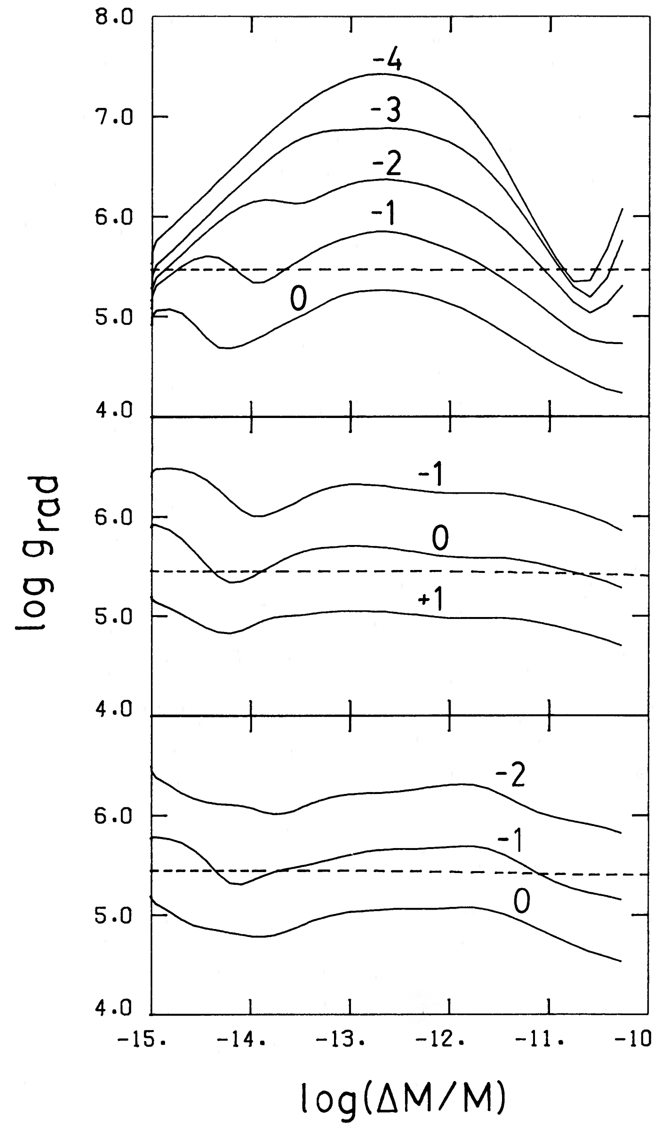

FIG. 9.—Radiative accelerations as a function of depth in (*top to bottom*) silicon, nitrogen, and carbon in a model at T_e = 35,000 K, log g = 5.5. Each curve is labeled by the logarithm of the element abundance with respect to the solar abundance. These calculations are performed using the approximate NLTE treatment described in § III*c*. The horizontal dashed lines correspond to the values of the local gravity, uncorrected for the effects of the electric field.

since all available abundances were derived from chemical analyses which assume a homogeneous atmospheric composition. Ideally, abundance analyses should now be pursued in terms of models with inhomogeneous element distributions, a non-trivial task.

Instead, we approach this problem by asking the following question: what abundances would standard analyses, based on homogeneous models, yield for our theoretical models with inhomogeneous abundance profiles? Furthermore, are these abundances consistent with the observed trends described in § I? A preliminary, if crude, answer was provided by consideration of the monochromatic optical depth scale (Bergeron *et al.* 1987). We go one step further here by calculating synthetic spectra based on inhomogeneous equilibrium abundance distributions and comparing them with their counterparts based on homogeneous distributions. This approach is likely to be

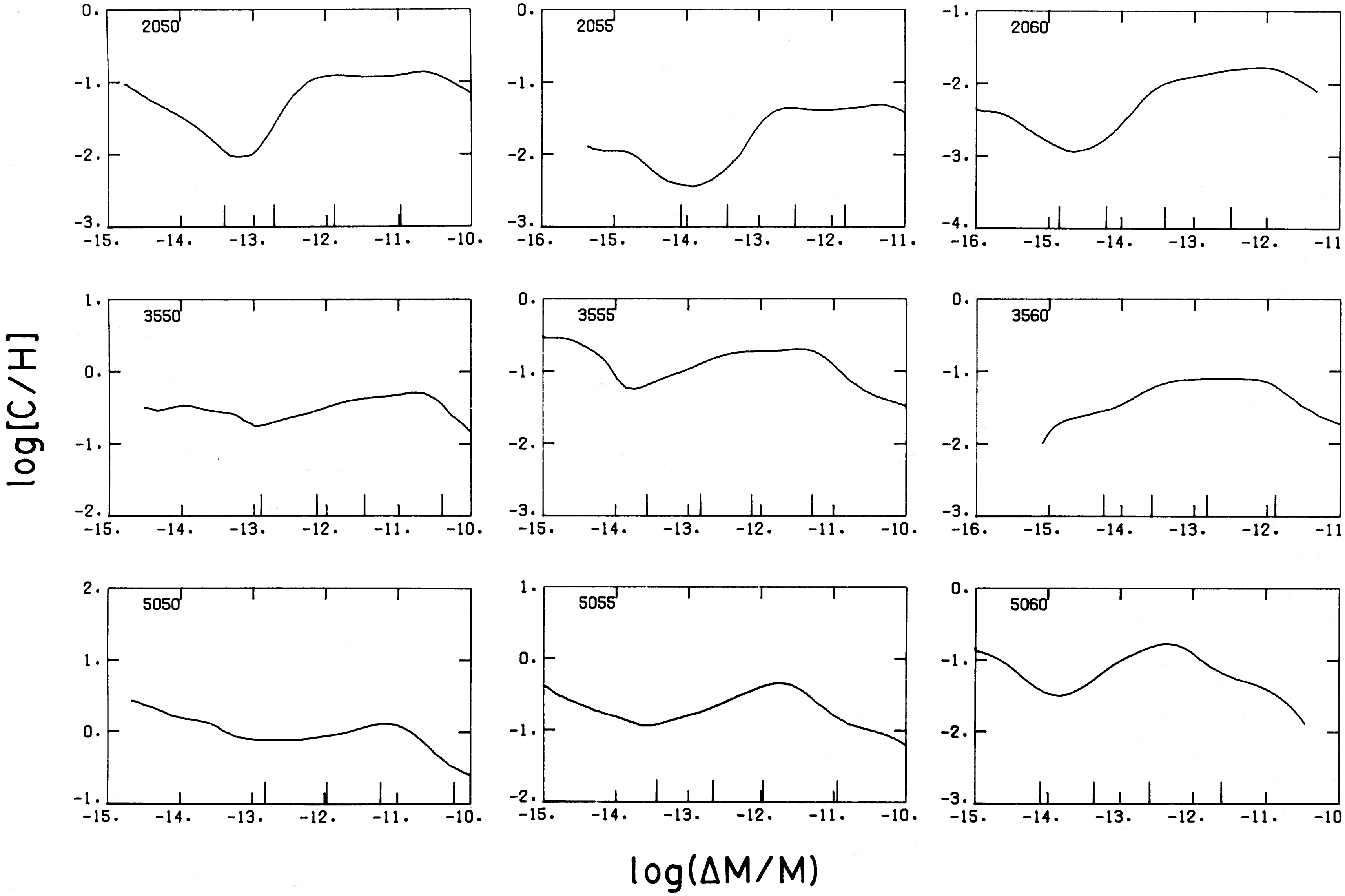

FIG. 10.—Equilibrium abundance profiles for carbon in the atmospheres of hot, hydrogen-rich subdwarfs using the approximate NLTE treatment described in § III*c*. Rosseland mean optical depths of 10^{-2}, 10^{-1}, 1, and 10 are indicated by long tick marks on the horizontal axis.

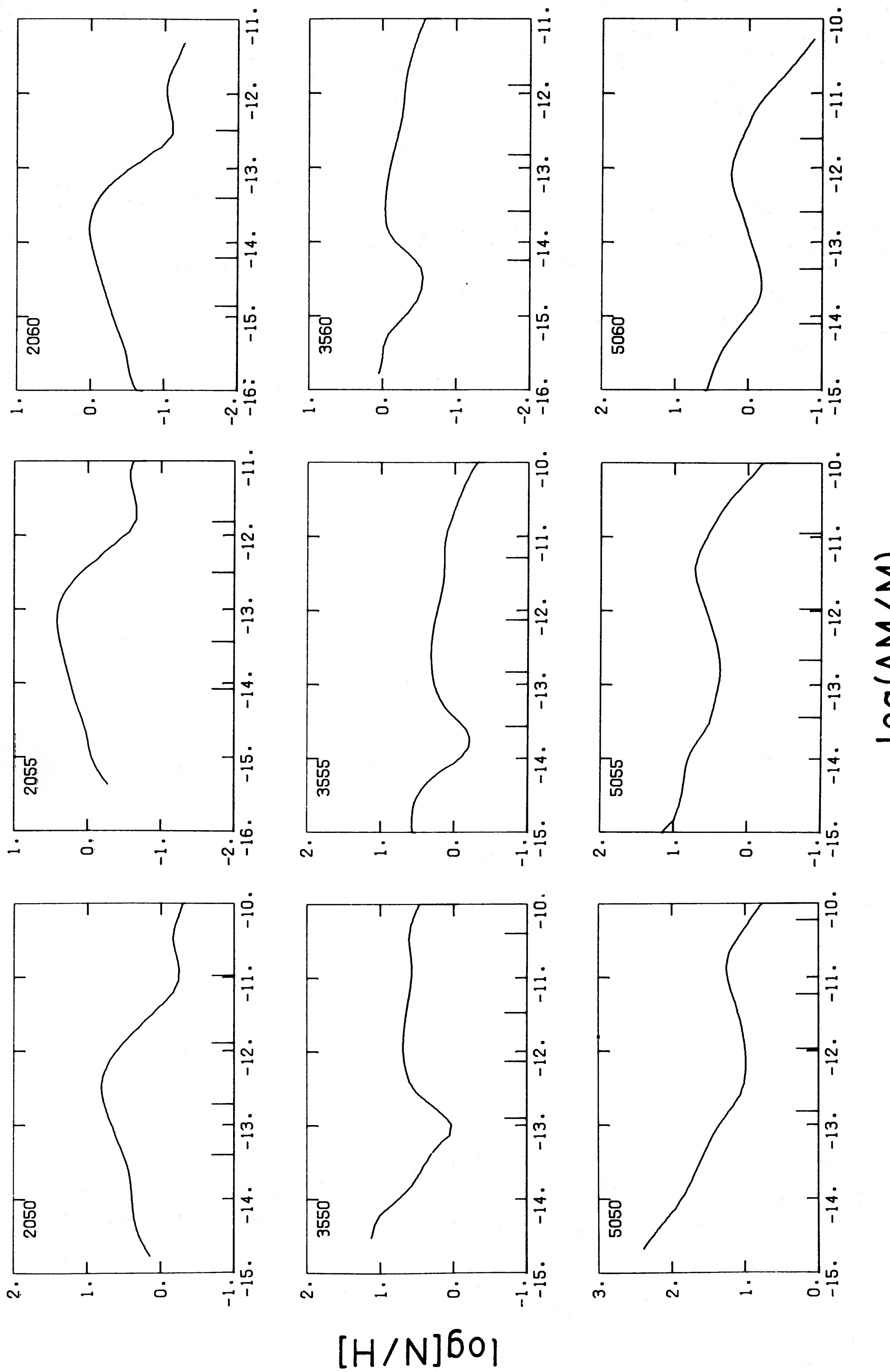

FIG. 11.—Same as Fig. 10, but for nitrogen

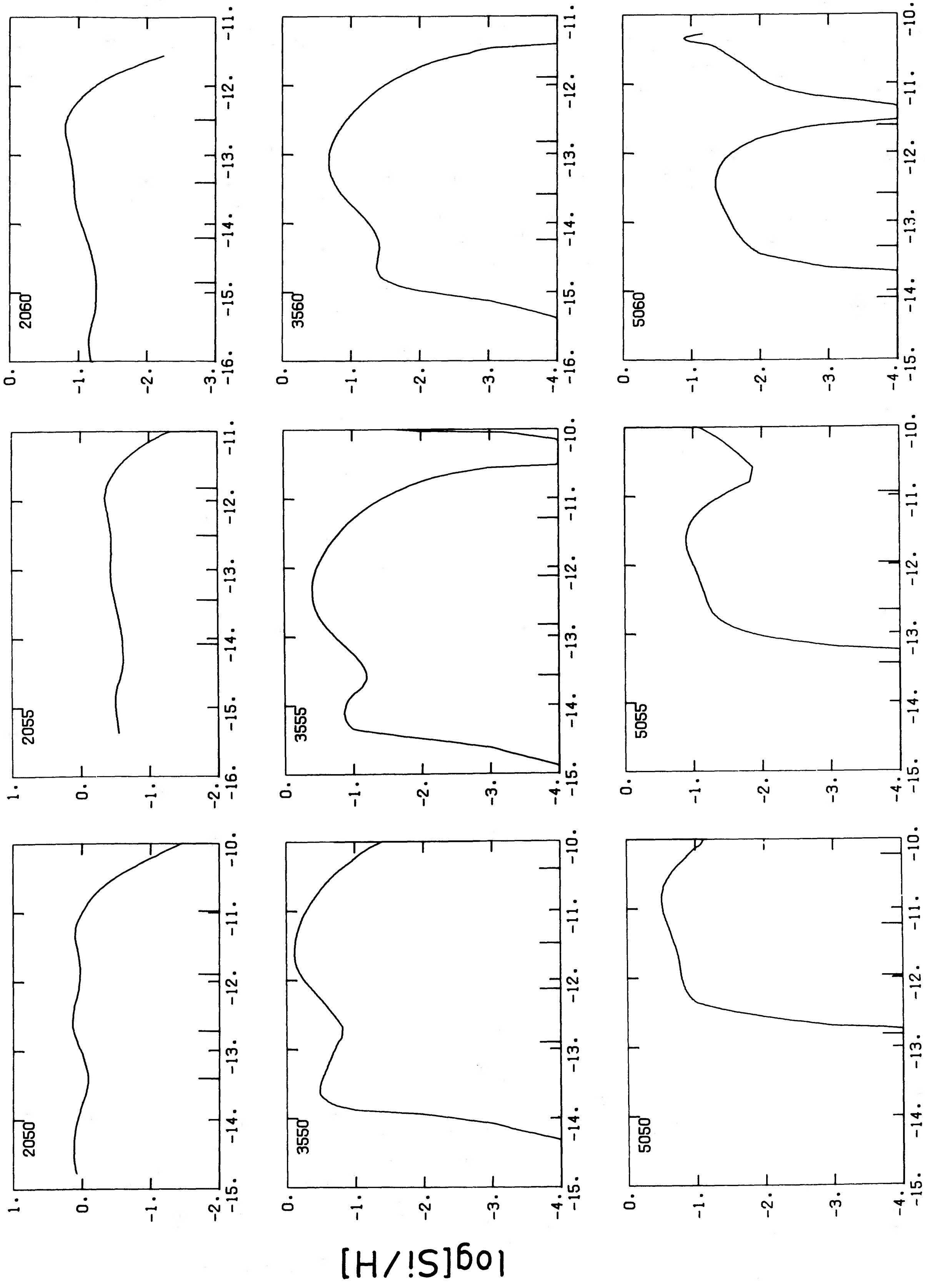

FIG. 12.—Same as Fig. 10, but for silicon

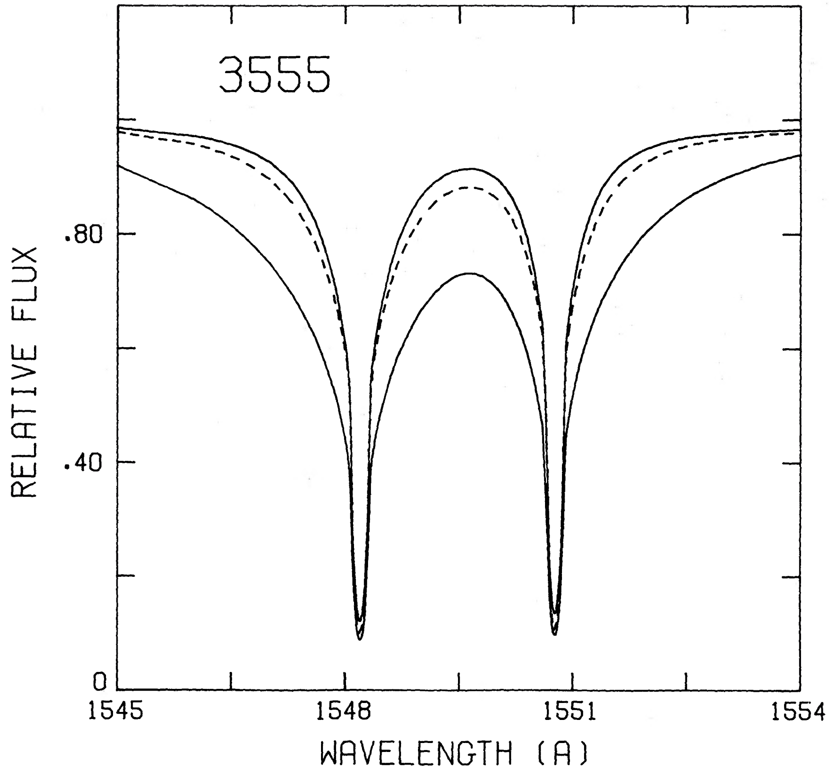

FIG. 13*a*

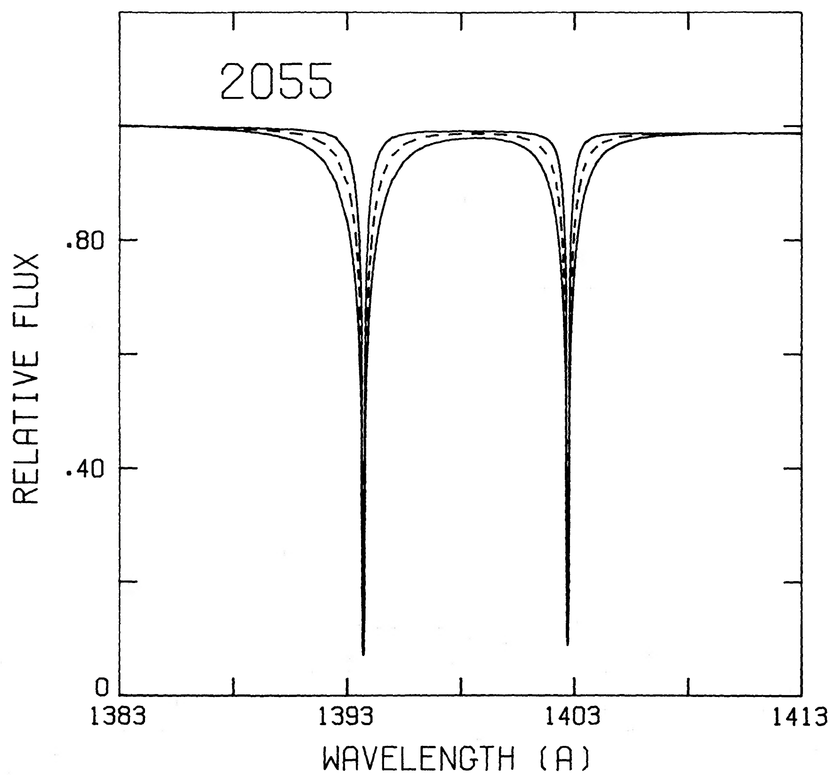

FIG. 13*b*

FIG. 13.—(*a*) Synthetic spectra in the region of the C IV resonance doublet for a model at $T_e = 35{,}000$ K, log $g = 5.5$. The dashed line indicates the results obtained with the equilibrium carbon distribution; the solid lines indicate results obtained with homogeneous carbon profiles at 10^{-1} and 10^0 the solar value. (*b*) Same as (*a*), but for the Si IV resonance doublet and a model at $T_e = 20{,}000$ K. (*c*) Same as (*b*), but for a model at $T_e = 30{,}000$ K. The solid lines indicate results obtained with homogeneous silicon profiles at 10^0 and $10^{0.5}$ the solar value. (*d*) Same as (*b*), but for a model at $T_e = 35{,}000$ K.

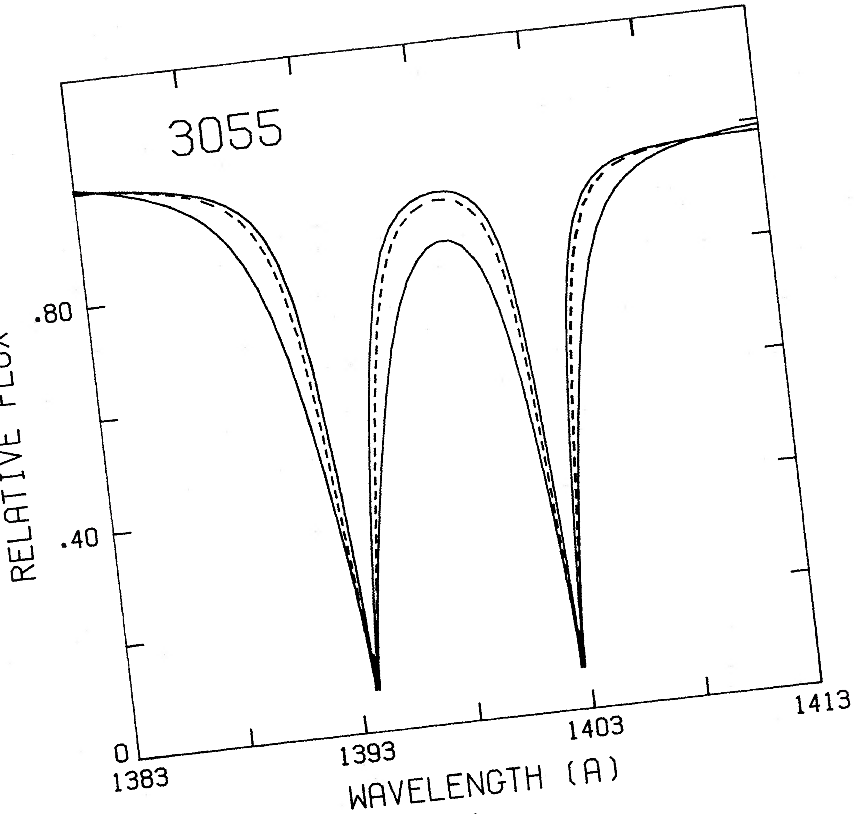

FIG. 13c

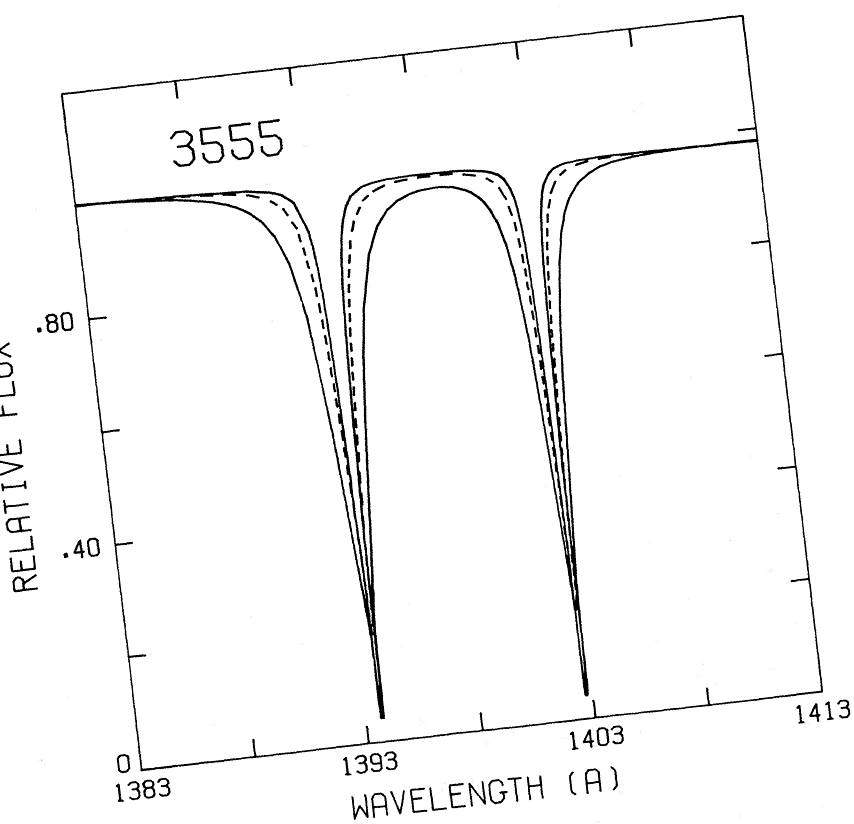

FIG. 13d

most useful for those elements, like silicon, which show steeply varying equilibrium profiles (see Fig. 12), and for which the depth of metal line formation may be somewhat more difficult to locate.

b) Some Illustrative Synthetic Spectra

The synthetic spectrum program used is described by Henry, Shipman, and Wesemael (1985) and has been used in previous studies of metal abundances in hot subdwarfs (Lamontagne *et al.* 1985; Lamontagne, Wesemael, and Fontaine 1987). In all cases, the theoretically computed equilibrium profiles is simply tacked onto a metal-free temperature and density stratification. The metals are thus uniformly treated in the trace approximation, as they are in our homogeneous models. Sample line profiles are presented in Figure 13. It should be noted, however, that, from an observational standpoint, line profile studies are limited by the quality of the often noisy *IUE* images and, for weaker lines, by the limited resolution of the instrument. In most cases, abundances have been derived from equivalent width analyses only.

We show, in Figure 13*a*, the C IV resonance doublet ($\lambda\lambda$1548.20, 1550.77) computed from our equilibrium abundance profile, together with profiles calculated for two homogeneous distributions all at T_e = 35,000 K, log g = 5.5. A star with such an inhomogeneous abundance profile would be assigned a homogeneous (C/H) abundance of the order of 0.2 the solar value. Not surprisingly, such an abundance could have easily been inferred from the rather flat equilibrium profiles of Figure 10, as it is characteristic of layers near $\tau_R \approx$ 0.1–1.

More interesting are the Figures 13*b–d*, where we show the Si IV resonance lines ($\lambda\lambda$1393, 1402) in three models covering a critical temperature range for that element, where the observed (Si/H) ratio varies by more than four orders of magnitude. All profiles from inhomogeneous models are bracketed by profiles based on homogeneous element distributions. Fits based on homogeneous distributions would all yield large (Si/H) ratios, (Si/H) $\gtrsim$ 0.1 the solar value *over the whole temperature range.* At this chosen gravity (log g = 5.5), the model at T_e = 30,000 K would even yield an *overabundance* of Si, were it to be interpreted with homogeneous models. These results are clearly at odds with the well-documented silicon deficiency above $\sim$27,000 K in hydrogen-rich subdwarfs, and their implications are now addressed below.

c) Astrophysical Implications of the Parameter-free Model

In the context of the parameter-free model which involves only radiative forces and gravitational settling, we have calculated equilibrium abundance distributions using radiative accelerations computed with an approximate treatment of the NLTE ionization balance required in the optically thin regions of the atmospheres. While a full NLTE calculation would be desirable, it would be surprising if it, or further refinements in the calculations of $g_{\rm rad}$, were to change the main conclusions reached here. Our estimates of $g_{\rm rad}$ in the line-forming region ($\tau_R \approx 0.1$) appears reliable enough, and a generalization of the conclusions of Paper I can already be drawn in the parameter-free context.

On the basis of the equilibrium abundance profiles of Figures 10–12, and of sample synthetic spectra such as those of Figure 13, the following statements can be made: in all models, carbon is found to be underabundant. For models of constant gravity, the amount of carbon supported increases with effective temperatures: this trend goes against that suggested by the observations, where the observed carbon abundance seems to decrease with increasing T_e. At T_e = 20,000 K, the predicted carbon abundance agrees with the observed values within the error bars but at T_e = 50,000 K, the predicted abundance is much too high.

For nitrogen, we find a much better agreement with the observational determinations: the nitrogen abundance is predicted almost solar, or occasionally slightly overabundant, *throughout* the effective temperature and gravity domain, as is observed.

It is in the case of silicon that the agreement with the parameter-free model is most unsatisfactory. At low effective temperatures, the latter predicts abundances between 1 and 0.1 the solar value. This abundance is somewhat higher than that observed, even when allowance is made for the error bars. For higher effective temperatures, underabundances by no more than a factor of $\sim$10 are predicted. These are a far cry from the deficiencies by factors at 10^4–10^5 which are observed in these stars, even when reasonable uncertainties are folded in: if $g_{\rm rad}$ were overestimated by a factor of 3 in the line-forming region, the equilibrium abundance of Si would be reduced by a factor of $\sim$10. The disagreement with the observational result would nevertheless remain. Near the transition temperature ($T_e \approx$ 30,000 K), the parameter-free model even predicts a small overabundance of silicon (see Fig. 13*d*)! The silicon results thus suggest that the parameter-free model is inadequate to reproduce the observed pattern of heavy elements in hot, hydrogen-rich subdwarfs.

This situation is, by now, a familiar one. It originally led Michaud *et al.* (1985)—on the basis of less overwhelming evidence—to suggest that additional transport processes, which might compete with diffusion, should be considered in hot subdwarf atmospheres. An argument was made for the plausible presence of a weak, otherwise undetectable, stellar wind. While much work remains to be done on the wind-model of Michaud *et al.*, it appears, at this stage, to offer an attractive alternative to the inadequate parameter-free model of equilibrium between upward radiative support and downward gravitational settling. Our most recent work (Michaud *et al.* 1988) suggests that such a parameter-free model is not likely to explain the helium abundance, however small, observed in hydrogen-rich subdwarfs. Future abundance studies of hot subdwarf atmospheres, coupled to detailed studies of particle transport processes, which *must* include the improved radiative forces terms presented here, may well thus provide us with a new probe of the physical state of the outer layers of these stars.

One of us (P. B.) is particularly grateful to J. Liebert for tactfully, but nevertheless eloquently, drawing his attention to inadequacies in an earlier presentation of these results. This work was supported in part by the NSERC Canada, and by the Fund F.C.A.R. (Québec). Computing funds were kindly provided by the Centre de Calcul of the Université de Montréal.

REFERENCES

Alecian, G., and Michaud, G. 1981, *Ap. J.*, **245**, 226.
Auer, L., and Mihalas, D. 1972, *Ap. J. Suppl.*, **24**, 205.
Baschek, B., Höfflich, P., and Scholz, M. 1982, *Astr. Ap.*, **112**, 76.
Baschek, B., Kudritzki, R. P., Scholz, M., and Simon, K. P. 1982, *Astr. Ap.*, **108**, 387.
Baschek, B., and Norris, J. 1975, *Ap. J.*, **199**, 694.
Bergeron, P., Wesemael, F., Michaud, G., and Fontaine, G. 1987, in *IAU Colloquium 95, The Second Conference on Faint Blue Stars*, ed. A. G. D. Philip, D. S. Hayes, and J. Liebert (Schenectady: L. Davis), p. 607.
Borsenberger, J., Michaud, G., and Praderie, F. 1979, *Astr. Ap.*, **76**, 287.
———. 1981, *Ap. J.*, **243**, 533.
———. 1984, *Astr. Ap.*, **139**, 147.
Chapelle, J., and Sahal-Bréchot, S. 1970, *Astr. Ap.*, **6**, 415.
Cox, A. N. 1965, in *Stars and Stellar Systems*, Vol. **8**, *Stellar Structure*, ed. L. H. Aller and D. B. McLaughlin (Chicago: University of Chicago Press), p. 195.
Cox, A. N., and Stewart, J. N. 1970, *Ap. J. Suppl.*, **19**, 243.
Gigas, D. 1986, *Astr. Ap.*, **165**, 170.
———. 1988, *Astr. Ap.*, **192**, 264.
Greenstein, J. L., and Sargent, A. I. 1974, *Ap. J. Suppl.*, **28**, 157.
Heber, U. 1986, *Astr. Ap.*, **155**, 33.
Heber, U., Hamann, W.-R., Hunger, K., Kudritzki, R. P., Simon, K. P., and Mendez, R. H. 1984*a*, *Astr. Ap.*, **136**, 331.
Heber, U., Hunger, K., Jonas, G., and Kudritzki, R. P. 1984*b*, *Astr. Ap.*, **130**, 119.
Henry, R. B. C., Shipman, H. L., and Wesemael, F. 1985, *Ap. J. Suppl.*, **57**, 145.
Kamp, L. W. 1973, *Ap. J.*, **180**, 447.
Kudritzki, R. P., Simon, K. P., Lynas-Gray, A. E., Kilkenny, D., and Hill, P. W. 1982, *Astr. Ap.*, **106**, 254.
Lamontagne, R., Wesemael, F., and Fontaine, G. 1987, *Ap. J.*, **318**, 844.
Lamontagne, R., Wesemael, F., Fontaine, G., and Sion, E. M. 1985, *Ap. J.*, **299**, 496.
Martel, G. 1973, M.Sc. thesis, Université de Montréal.
Michaud, G. 1977, *Highlights Astr.*, Vol. **4**, Part 2, p. 177.
———. 1986, in *IAU Colloquium 87, Hydrogen-Deficient Stars and Related Objects*, ed. K. Hunger, D. Schönberner, and N. K. Rao (Dordrecht: Reidel), p. 453.
Michaud, G. 1987*a*, in *IAU Colloquium 90, Upper Main Sequence Stars with Anomalous Abundances*, ed. C. R. Cowley, M. M. Dworetsky, and C. Megessier (Dordrecht: Reidel), p. 459.
———. 1987*b*, *Phys. Scripta*, **36**, 112.
Michaud, G., Bergeron, P., Heber, U., and Wesemael, F. 1988, *Ap. J.*, submitted.
Michaud, G., Bergeron, P., Wesemael, F., and Fontaine, G. 1985, *Ap. J.*, **299**, 741 (Paper I).
Michaud, G., Charland, Y., Vauclair, S., and Vauclair, G. 1976, *Ap. J.*, **210**, 447 (MCVV).
Mihalas, D. 1978, *Stellar Atmospheres* (2d ed.; San Francisco: Freeman).
Milne, E. A. 1927, *M.N.R.A.S.*, **87**, 697.
Montmerle, T., and Michaud, G. 1976, *Ap. J. Suppl.*, **31**, 489.
Moore, C. E. 1949, *Atomic Energy Levels* (Washington: US Government Printing Office) (NBS Pub. 467), Vol. 1.
Paczyński, B. 1969, *Acta Astr.*, **19**, 1.
Paquette, C., Pelletier, C., Fontaine, G., and Michaud, G. 1986, *Ap. J. Suppl.*, **61**, 197.
Sahal-Bréchot, S., and Segre, E. R. A. 1971, *Astr. Ap.*, **13**, 161.
Shipman, H. L. 1987, in *IAU Colloquium 95, The Second Conference on Faint Blue Stars*, ed. A. G. D. Philip, D. S. Hayes, and J. Liebert (Schanactady: L. Davis), p. 273.
Vauclair, G., and Liebert, J. 1987, in *Exploring the Universe with the IUE Satellite*, ed. Y. Kondo (Dordrecht: Reidel), p. 355.
Vauclair, G., Vauclair, S., and Greenstein, J. L. 1979, *Astr. Ap.*, **80**, 79.
Vauclair, S., Michaud, G., and Charland, Y. 1974, *Astr. Ap.*, **31**, 381 (VMC).
Wesemael, F., Auer, L. H., Van Horn, H. M., and Savedoff, M. P. 1980, *Ap. J. Suppl.*, **43**, 159.
Wesemael, F., Winget, D. E., Cabot, W., Van Horn, H. M., and Fontaine, G. 1982, *Ap. J.*, **254**, 221.
Wiese, W. L., Smith, M. W., and Glennon, B. M. 1966, *Atomic Transition Probabilities*, Vol. **1** (NSRDS-NBS 4).
Wiese, W. L., Smith, M. W., and Miles, B. M. 1969, *Atomic Transition Probabilities*, Vol. **2** (NSRDS-NBS 22).
Winget, D. E., and Cabot, W. 1980, *Ap. J.*, **242**, 1166.

P. Bergeron, G. Fontaine, G. Michaud, and F. Wesemael: Département de Physique, Université de Montréal, C.P. 6128, Succ. A, Montréal, Québec, Canada H3C 3J7